Journal of Solid State Electrochemistry (2018) 22:1091–1098
https://doi.org/10.1007/s10008-017-3851-5

ORIGINAL PAPER

Influence of the surface mechanical attrition treatment (SMAT) on the corrosion behavior of Co28Cr6Mo alloy in Ringer's solution

D. V. Tchana Nkonta[1,2] · F. Simescu-Lazar[1] · R. Drevet[1] · O. Aaboubi[1] · J. Fauré[1] · D. Retraint[2] · H. Benhayoune[1]

Received: 18 May 2017 / Revised: 5 October 2017 / Accepted: 28 November 2017 / Published online: 7 December 2017

Abstract

The low carbon Co28Cr6Mo alloy used for artificial joints like hip and knee prostheses is subjected to a surface treatment called SMAT (surface mechanical attrition treatment). The purpose of this treatment is to modify the surface mechanical properties of the treated alloy. Since the SMAT impacts the surface of materials, its influence on the corrosion behavior of the CoCrMo alloy has to be assessed in a physiological solution as Ringer's solution. Furthermore, a specific biomedical polishing is coupled with the SMAT in order to finalize the production of a hip prosthesis ready for use. The corresponding corrosion behavior is also studied. The corrosion behavior of CoCrMo alloy samples is investigated using electrochemical techniques (potentiodynamic polarization measurements and electrochemical impedance spectroscopy (EIS)) in physiological liquid and simulated by an equivalent circuit. The polarization results show the reduction of the corrosion current density and the increase of the corrosion potential after the SMAT. The EIS analyses also show the benefit of the SMAT on the corrosion resistance of the CoCrMo alloy. The surface morphology modification and the phase's transformation induced by the SMAT are evaluated by scanning electron microscopy (SEM) and X-ray diffraction (XRD).

Keywords Corrosion · CoCrMo alloys · SMAT · Polarization · EIS · Biomedical polishing

Introduction

In recent years, the number of patients who need an orthopedic implant has considerably increased. Consequently, the total hip arthroplasty has been developed, becoming one of the most successful surgical procedures. The materials used for orthopedic implants play a very important role in implants fixation. The choice of material strongly influences the rigidity, the corrosion characteristics, the biocompatibility, and the tissue receptivity of the implant [1–4].

The most used materials in orthopedics applications are surgical grade pure titanium (Ti), Ti alloys, cobalt-chromium alloys, and stainless steels [5–7]. Among these alloys, stainless steel has less interesting corrosion and mechanical properties for a permanent implant application [8]. Before the use of titanium, the cobalt-based alloys had largely replaced stainless steel as materials for permanent implants due to their higher wear resistance [6]. These properties justify the choice of the Co28Cr6Mo alloy for the fabrication of the head of the hip implant. Indeed, this part of the implant exhibits high strength and ductility.

Despite the high mechanical performances of the CoCrMo alloy, clinical research has shown the presence of cobalt and chromium ions in the urine of patients with a total hip replacement in CoCrMo. The metal ion release inside the human body during the corrosion process can cause adverse tissue reactions and the premature failure after a total hip arthroplasty [9]. Pains and risks of cancer are also possible for the patient. For these reasons, the corrosion behavior of implanted materials remains a persistent challenge in orthopedic surgery.

However, some studies show that the optimization of material microstructure and mechanical properties by means of surface modification techniques, such as surface mechanical attrition treatment (SMAT) [10], ultrasonic shot peening [11], high energy shot peening (HESP) [12], extrusion [13], and cryogenic burnishing [14], can improve the corrosion behavior of materials [15]. For example, the SMAT introduces

✉ H. Benhayoune
hicham.benhayoune@univ-reims.fr

[1] LISM EA 4695, Université de Reims Champagne-Ardenne, Bat. 6, Moulin de la Housse, BP 1039, 51687 Reims Cedex 2, France

[2] LASMIS, UMR STMR CNRS 6281, Université de Technologie de Troyes, 12 rue Marie Curie, 10100 Troyes Cedex, France

localized plastic deformation, allowing the grains refinement without any change of the chemical composition. This mechanical treatment is known to modify the surface of materials by inducing changes of the mechanical properties and of the crystallographic structure.

Until today, the SMAT has been successfully performed on some materials such as 304-316-409 stainless steel [16–18], titanium alloy [10, 19], and cobalt-based alloy [20, 21]. The results show that the effect of the SMAT on the corrosion resistance depends on the nature of the alloy and on the mechanical treatment parameters.

In the present investigation, a low carbon CoCrMo alloy was treated by the SMAT. The objective of this work was to investigate the effect of the SMAT on the corrosion behavior of CoCrMo alloy in Ringer's solution. On the other hand, metallic articular bearing surfaces are systematically polished to produce low coefficients of friction [22]. Therefore, in the present work, the influence of a biomedical polishing was also investigated.

The material surface was characterized by using X-ray diffraction (XRD) and scanning electron microscopy (SEM).

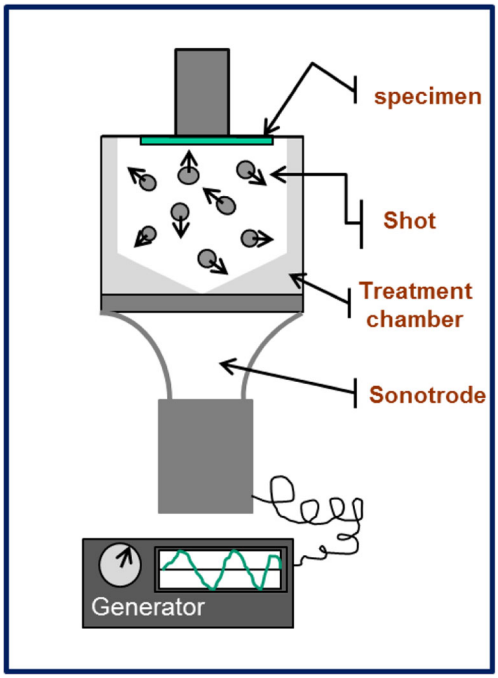

Fig. 1 Sketch of the SMAT process

Experimental

Materials

The material used for the present study is a low carbon Co28Cr6Mo alloy (CRITT-MDTS, Charleville-Mézières, France). This material is suitable for medical applications, and its chemical composition complies with the international standard ISO 5832-12 (64.5 wt% Co, 27.6 wt% Cr, 5.5 wt% Mo, 0.8 wt% Mn, 0.6 wt% Si, 0.45 wt% Fe, 0.3 wt% Ni, 0.16 wt% N, 0.05 wt% C, 0.02 wt% W, 0.01 wt% Cu, 0.003 wt% P, and 0.0005 wt% S). For all experiments, the CoCrMo alloy was machined into disc specimen with a 50-mm diameter and 6-mm thickness.

Mechanical treatment and sample preparation

Before each mechanical treatment, the CoCrMo alloy was prepared using silicon carbide (SiC) papers of 800 and 1200 grit followed by an ultrasonication with acetone and high-purity water. Two mechanical treatments were applied: the SMAT and the biomedical polishing.

SMAT

The CoCrMo alloy was subjected to SMAT during 15 min with 3-mm diameter balls in 100Cr6 alloy.

Figure 1 presents the experimental setup of the SMAT process. The parameters controlling the process are the balls' diameter, the vibration frequency, the processing time, and the vibration amplitude. The vibration was generated by a sonotrode with a vibration frequency of 20 kHz. The distance between the sample and the sonotrode was fixed at 17 mm. When the balls are in resonance, the sample surface is impacted by a large number of flying balls during a short period of time. The flying directions of the balls inside the vibration chamber are random. Each ball induces several repeated multidirectional plastic deformations in the surface layer of the sample. In this condition, the plastic deformation mechanism of the CoCrMo alloy impacts about 10 μm in depth [23, 24].

Biomedical polishing

Before and after the SMAT, the samples were subjected to a biomedical polishing to reduce the surface roughness following the biomedical standard (arithmetic roughness $R_a <$ 0.5 μm). The biomedical polishing based on brush polishing method was performed by MARLE® orthopedics manufacturing company. For reasons of confidentiality and intellectual property, the steps of this treatment could not be detailed.

In this work, four CoCrMo samples were used for the corrosion tests and labeled according to their surface treatment. The sample noted (W) was obtained by cutting the CoCrMo alloy followed by a polishing step using silicon carbide (SiC) papers of 120, 600, and 1200 grit. For the second sample noted (W-P), a biomedical polishing (P) was realized on the (W) surface. The samples named (S15) are (W) discs subjected to the SMAT for 15 min, and those noted (S15-P) are (S15) discs with biomedical polishing (P).

X-ray diffraction

The phase's transformations induced during the treatments were determined by X-ray diffraction (XRD) measurements using an X-ray diffractometer (Bruker D8 Advance). The X-ray pattern data was collected from $2\theta = 35$ to 90° using a monochromatic $Cu_{K\alpha}$ radiation with a step of 0.06° every 10 s. The Powder Diffraction Files (PDF) of the International Center for Diffraction Data (ICDD) were used for the phase's identification.

Scanning electron microscopy

A LaB_6 scanning electron microscope (JEOL JSM-6460 LV) operating at 0–30 kV was used to observe the surface topography of the untreated and treated CoCrMo samples.

Electrochemical corrosion testing

The corrosion behavior of the untreated CoCrMo alloy and that of those subjected to a mechanical treatment was evaluated by potentiodynamic polarization and electrochemical impedance spectroscopy (EIS). The potentiodynamic polarization tests were performed by scanning the applied potential from − 1.5 V vs SCE (saturated calomel electrode) to 0.8 V vs SCE with a scan rate of 1 mVs^{-1}. Before testing, the samples were allowed to reach the open circuit potential E_{OCP} for 15 min. Each test was repeated four times in order to reduce the margins of error and to verify the repeatability of results. The impedance measurements were carried out after 15 min at open circuit potential (OCP) using a PGZ potentiostat RADIOMETER 100. The frequency ranges from 10 kHz to 10 mHz with five points per decade and an amplitude of 10 mV. The impedance data was modeled using the ZView software.

The electrolyte used for the electrochemical corrosion measurements was Ringer's solution purchased from Merck (9.000 g L^{-1} NaCl, 0.200 g L^{-1} $NaHCO_3$, 0.420 g L^{-1} KCl, 0.480 g L^{-1} $CaCl_2$). The physiological liquid is a saline solution (pH = 7.00 ± 0.02 at 25 °C) without vitamins and amino acids [25]. The temperature of the electrolyte was maintained at 37 °C during the experiments.

Results and discussion

XRD analysis

The X-ray diffraction patterns of the CoCrMo alloy before and after the mechanical treatments are presented in Fig. 2. The W and W-P samples reveal the presence of two phases: the austenite (γ-fcc) and the martensite (ε-hcp). These two diffraction patterns are quite similar which clearly indicates that the biomedical polishing does not generate any crystallographic transformation of the alloy.

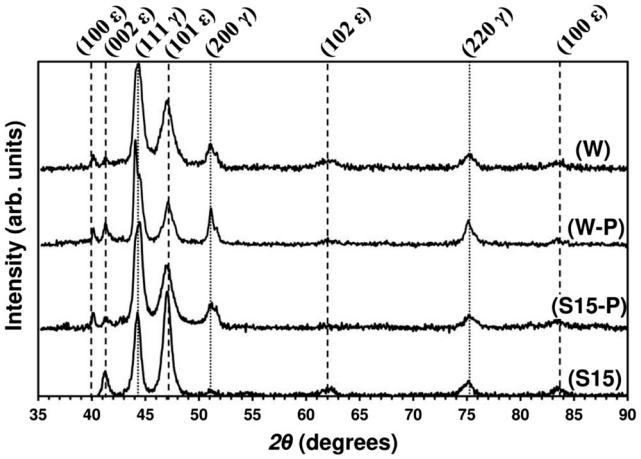

Fig. 2 X-ray diffraction patterns of the four CoCrMo alloys

The SMAT of the CoCrMo alloy (S15) has resulted in a decrease in the intensity of the (111 γ) and (200 γ) peaks and an increase in the intensity of the (101 ε) peak. This result clearly shows that the martensitic phase (ε-hcp) is generated at the surface of the CoCrMo alloy during the SMAT. Moreover, the biomedical polishing does not affect the martensitic transformation since the (101 ε) peak intensity in the case of the S15-P sample is greater than that of the W-P sample.

These results have been observed previously in literature in the case of AISI 304 stainless steel [16] and cobalt [26]. The mechanism of phase transformation was attributed to the increase in stacking-fault energy generated by the deformations. Wu et al. [26] have studied the grain refinement and the strain accommodation in cobalt (a mixture of hexagonal close packed (hcp) and face-centered cubic (fcc) phases) subjected to the SMAT. They observed a strain accommodation in the fcc phase started by the slip of dislocations at low strain, forming intersecting planar arrays of dislocations. With increasing strain, the $\gamma \rightarrow \varepsilon$ transformation occurred and contributed to the grain refinement.

SEM observations

Figure 3 shows the surface morphology of the four CoCrMo samples. The surface of W sample (Fig. 3a) shows stripes generated by the SiC polishing. These stripes are still slightly visible despite the biomedical polishing (Fig. 3b). After the SMAT, the surface of the S15 sample (Fig. 3c) is chaotic and rough but the biomedical polishing (S15-P) has significantly reduced its surface roughness and only residual stripes and ball impacts remain visible (Fig. 3d). The roughness (R_a) was measured using a contact roughness tester. Its value has increased from about 0.02 to 0.64 μm after the SMAT (S15 sample). After the biomedical polishing, it has decreased to around 0.30 μm (S15-P sample).

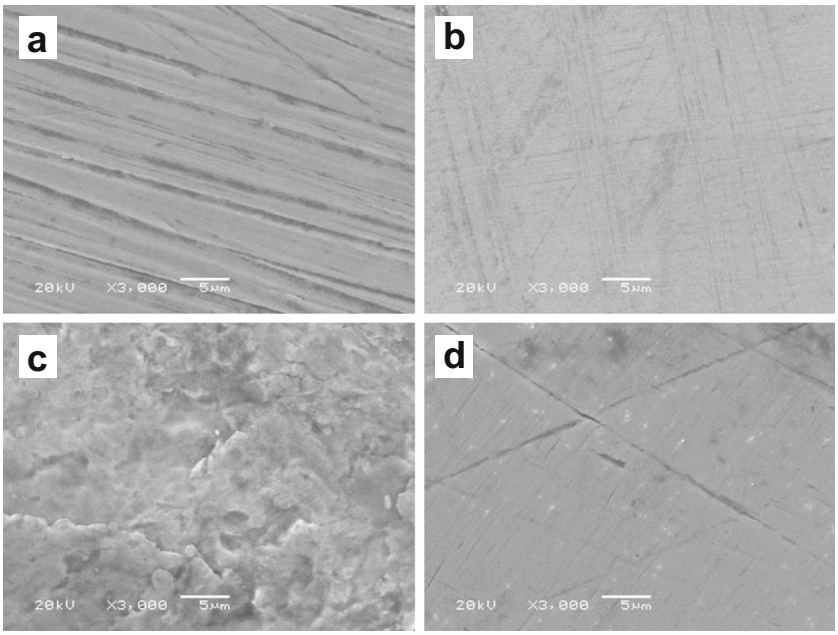

Fig. 3 SEM surface morphology of the CoCrMo alloys. **a** W. **b** W-P. **c** S15. **d** S15-P

Electrochemical corrosion testing

Polarization curves

The potentiodynamic polarization is used to compare the dynamic electrochemical responses of the four CoCrMo alloy surfaces. This characterization aims at determining the influence of each treatment step on the corrosion behavior of the CoCrMo alloy. Figure 4 shows typical Tafel polarization curves for the four CoCrMo samples in Ringer's solution. These curves were obtained after stabilization of the open circuit potential during 15 min (results not shown).

In the cathodic branch, the hydrogen evolution reaction (HER) due to the electrolysis of water appears from − 1.5 V vs SCE to − 0.9 V vs SCE. Moreover, the oxygen reduction reaction (ORR) also occurs since the electrochemical experiment is carried out at open room atmosphere in a non-deaereted physiological solution. The anodic branch of the curves describes a typical behavior of metals that undergo a passivation when they are exposed to an appropriate electric current density. The formation of a passive oxide film on the sample surface inhibits the corrosion evolution, resulting in the formation of a plateau on the Tafel curves. For example, the polarization curve of the W sample shows a wide plateau from − 0.75 V vs SCE to 0.50 V vs SCE with a current density of about 10^{-1} mA cm^{-2}. This plateau corresponds to the passivation of the alloy surface. Thus, the corrosion reactions are reduced and both active and passive behaviors occur. Next, the transpassive region is reached (no more passivation) where the current density increases with the applied potential. The corrosion current densities (i_{corr}) can be determinate by extrapolating the linear part of the cathodic and anodic curves to the open circuit potential (E_{OCP} vertical axis) [27]. The corrosion parameters deduced from these curves are reported in Table 1. We note that the corrosion current densities (i_{corr}) and the corrosion potentials (E_{corr}) for W and W-P samples are almost the same. Thus, the corrosion behavior of the CoCrMo alloy was not improved by the biomedical polishing.

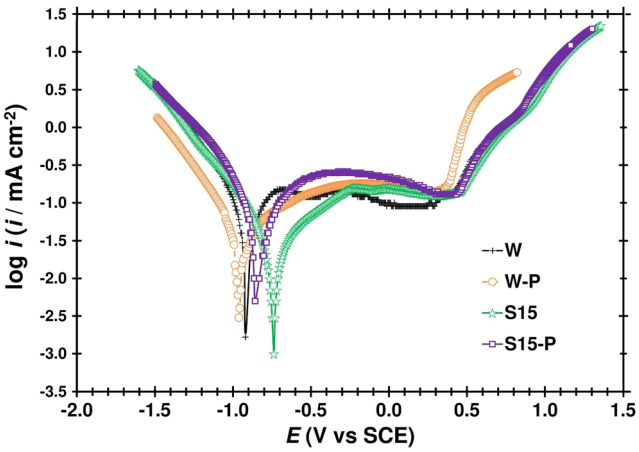

Fig. 4 Tafel curves of the four CoCrMo alloys in Ringer's solution (scan rate 1 mV s^{-1})

Table 1 Corrosion parameters extracted from the polarization curves

CoCrMo samples	E_{corr} (mV vs SCE)	i_{corr} (μA cm^{-2})
W	− 920 ± 90	23.5 ± 2.4
W-P	− 962 ± 90	25.2 ± 2.6
S15	− 737 ± 70	9.3 ± 1.0
S15-P	− 858 ± 80	21.3 ± 2.2

For the S15 sample, the corrosion potential (E_{corr}) increases from − 0.920 V vs SCE to − 0.737 V vs SCE and the corrosion current density (i_{corr}) is divided by about 2.5 in comparison with the W sample. These results indicate that the passive film formed on the CoCrMo alloy surface after the SMAT is more protective. The improved surface passivity can be attributed to the surface changes generated by the SMAT. Indeed, the chemical composition of the passive layer plays an important role in the protection against corrosion. This layer is generally composed of metal oxides. For example, Hao et al. have shown that the passive layer rich in chromium oxides formed after SMAT of 316L stainless steel improves the resistance to the attack of corrosive chloride anions [17]. Balusamy et al. have studied the effect of SMAT on AISI 409 stainless steel and explain that it improves the corrosion resistance through the formation of a passive film associated with surface nanocrystallization [18]. Jelliti et al. studied the effect of SMAT on the TA6V alloy and showed that the improvement of the corrosion resistance in Ringer's solution is due to the formation of a passive layer rich in titanium oxides [19]. Concerning the CoCrMo alloy, Petrov et al. have clearly shown that a surface treatment similar to SMAT leads to the formation of a passive layer consisting essentially of cobalt oxides (determined by XPS analysis) [20]. Combined with the martensitic transformation, this layer allows an improvement of the corrosion resistance in a medium similar to Ringer's solution. In our case, we can consider that the same mechanisms take place. According to Petrov et al., the severe plastic deformation of the surface alloy promotes an intense penetration of oxygen atoms into the crystal lattices leading to the formation of the oxide passive film. At the same time, the formation of interfacial boundaries associated with high fraction of grains with (111)γ and (0002)ε planes parallel to the surface of the alloy promotes enhanced corrosion resistance.

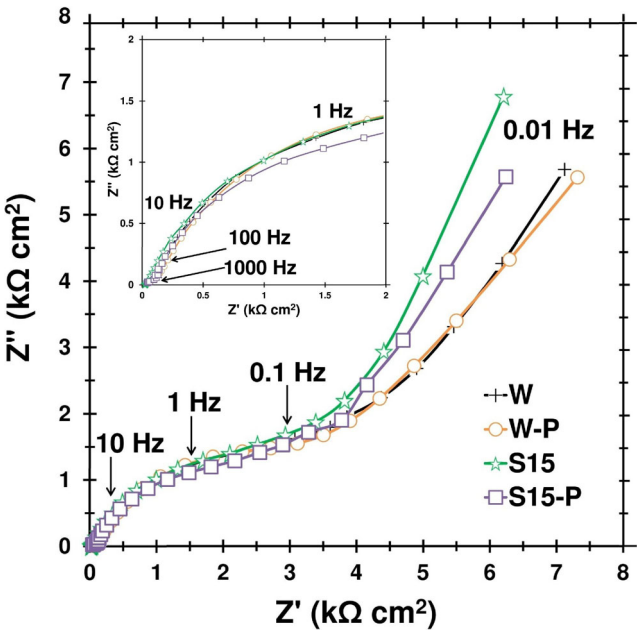

Fig. 5 Nyquist plot of the four CoCrMo alloys immersed in Ringer's solution

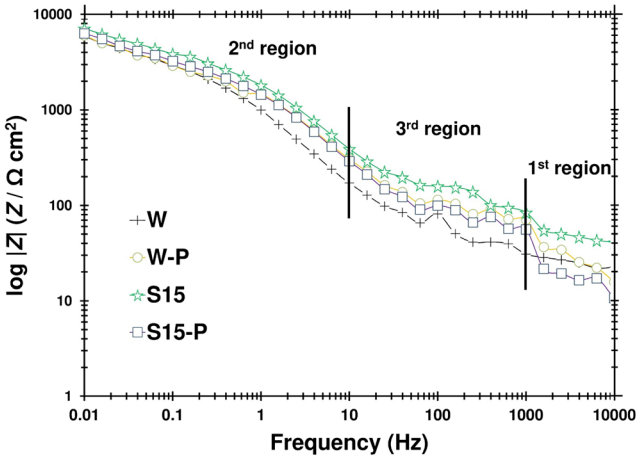

Fig. 6 Bode impedance plot of the four CoCrMo alloys immersed in Ringer's solution

Moreover, after the biomedical polishing, the E_{corr} of S15-P slightly increases (from − 0.962 V vs SCE to − 0.858 V vs SCE) and the i_{corr} slightly decreases (from 25.2 to 21.3 μA cm^{-2}) in comparison with the W-P sample. This indicated that the biomedical polishing does not alter the advantages of the surface passivation generated by the SMAT.

Electrochemical impedance spectroscopy

The EIS is used to get information on the characteristics of the passive films and on the nature of the electrochemical processes occurring at the surface of the alloy in the physiological medium.

The Nyquist diagrams obtained for the four CoCrMo samples are shown in Fig. 5. It is observed the presence of an incomplete semi-circle in the high-frequency region with a larger diameter for the S15 sample. After biomedical polishing

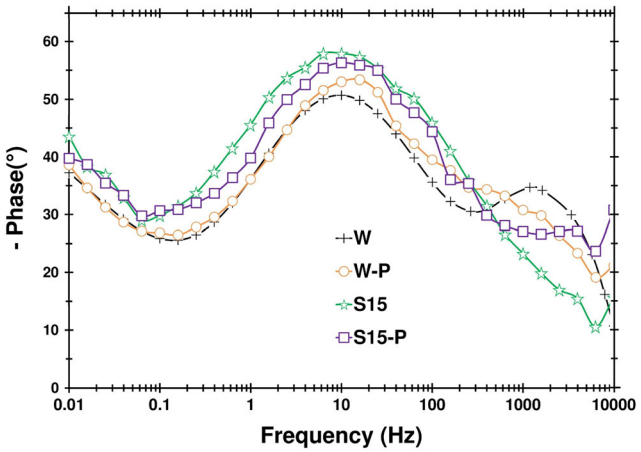

Fig. 7 Bode phase plot of the four CoCrMo alloys immersed in Ringer's solution

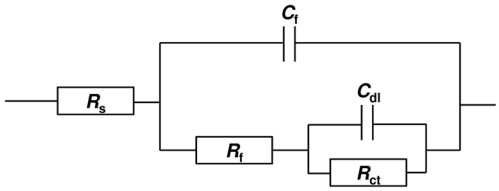

Fig. 8 Equivalent circuit used to model the EIS data of the CoCrMo alloys

(S15-P), the diameter of the semi-circle remains greater than that of the W and W-P samples. The incomplete semi-circle observed on the Nyquist diagram highlights the charge transfer reactions between the sample surface and the electrolyte [21]. The increase of the semi-circle diameter indicates the enhancement of the passive film stability. The largest semi-circle diameter in the case of S15 and S15-P samples shows the noblest electrochemical behavior induced by the SMAT of the CoCrMo alloy.

The Bode impedance plots (Fig. 6) can be divided in three regions; each one reveals specific information on the electrochemical process at the surface of the CoCrMo alloy. In the first region (high frequencies (1000 Hz $< f <$ 10,000 Hz), we observe that log $|Z|$ forms a plateau with a weak slope. There is also a sharp fall of the phase values in this area (Fig. 7). These results describe a typical response of a resistive behavior of the electrolyte which is more highlighted in the case of S15 and S15-P samples.

The second region (low frequencies 10^{-2} Hz $< f <$ 10 Hz) generally provides information about the passive behavior of the material. In this area, we can observe that log $|Z|$ shows a linear tendency which describes the character of a passive film on the surface of the material [18]. At 10^{-2} Hz, the log $|Z|$ of the S15 sample reaches a higher value (~ 7000 Ω cm^2) than the W sample (~ 6000 Ω cm^2). These results show that the SMAT can generate a more efficient passive layer, improving the CoCrMo alloy behavior against corrosion in physiological medium.

In the third region (middle frequencies 10 Hz $< f <$ 10^3 Hz), the maximum peak observed on the phase plot (Fig. 7) may indicate the formation of a passive film or its evolution [28, 29]. This peak is maximum for the S15 sample, confirming that the SMAT promotes the CoCrMo alloy passivation.

The Bode phase diagrams in Fig. 7 show two time constants: one at low frequency (in the first region) and the second at the interface second region/third region corresponding to relaxation times. These results suggest that the passive film formed on the CoCrMo surface is made of two layers: the inner dense passive layer and the outer porous layer [28, 30].

Furthermore, the phase angles for all the samples are lower than 90°, indicating that the CoCrMo alloy behavior does not correspond to that of an ideal capacitor. To explain the distribution of relaxation times resulting from surface heterogeneities, the formation of passivation films and the adsorption of species, a model of the sample/electrolyte, is necessary. The equivalent electrical circuit proposed for the different samples is given in Fig. 8. R_s corresponds to the electrolyte resistance; C_{dl} and R_{ct} represent the double layer capacitance and the charge transfer resistance at the CoCrMo sample/electrolyte interface. Particularly, R_{ct} quantifies the impact of the experimental conditions on the kinetics of the oxidation reaction during the corrosion process given by

$$M \rightarrow M^{z+} + z\, e^{-}$$

M is a metallic atom of the alloy surface.

C_f and R_f are the capacitance and the resistance of the passive film. The global values of the polarization resistance R_p are calculated from the values of R_f and R_{ct} by the following relationship: $R_p = R_f + R_{ct}$.

As an illustration, Figs. 9 and 10 present the comparison between the experimental values and the calculated data obtained from this model in the case of S15 and S15-P samples. A good agreement is obtained, and the electrochemical

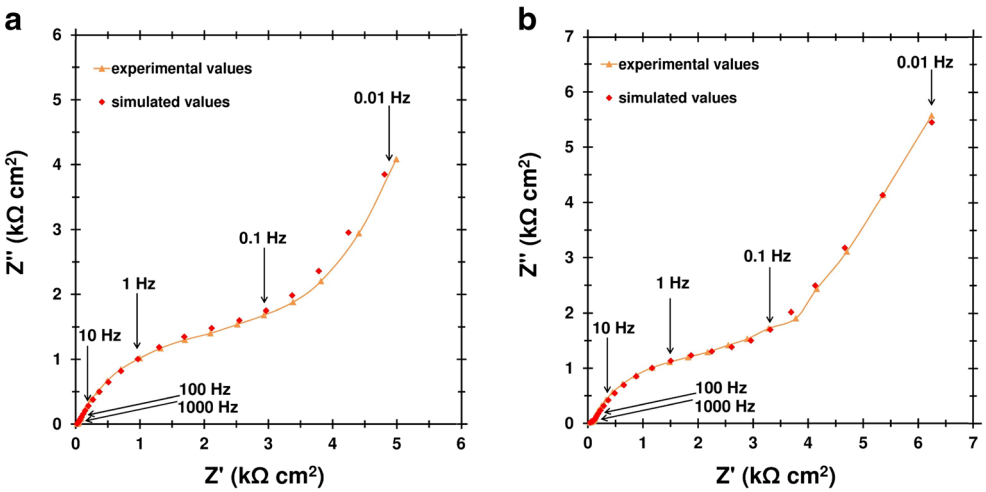

Fig. 9 Experimental and simulated Nyquist diagrams of the CoCrMo alloys. **a** S15. **b** S15-P

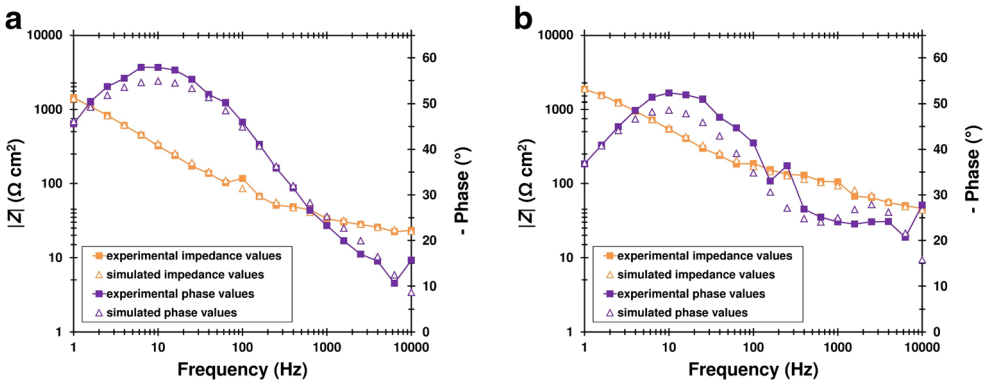

Fig. 10 Experimental and simulated Bode impedance and phase diagrams of the CoCrMo alloys. **a** S15. **b** S15-P

characteristics identified from the equivalent electrical circuit for all the samples are summarized in Table 2.

All of these corrosion results indicate that the chloride ions in the Ringer's solution induce a competition between the local formation and the destruction of the passive film formed on the surface of the different CoCrMo samples. This corrosion mechanism leads to the charge transfer resistance R_{ct} decrease and to the double layer capacitance C_{dl} increase during immersion in Ringer's solution. It can be noticed that for the S15 sample, the R_{ct} value remains higher than that of the W sample. R_f is the electrical resistance of ion transfer through the passive film pores, its value is maximum for the S15 and S15-P samples. The R_f value evolution indicates that the electrolyte diffusion into the passive film pores is maximum in the case of W and W-P samples while it is strongly reduced after the SMAT because of the surface grains refinement.

On the other hand, the capacitance of the passive film C_{dl} formed on the S15 surface is approximately twice lower than that of the W sample. This result shows that the SMAT reduces the active surface area and increases the thickness of the passive film. Compared with the W sample, the formation of this passive film in the case of S15 sample leads to a better protection of the CoCrMo alloy in Ringer's solution, as shown by the EIS diagrams [12, 26]. Indeed, the SMAT process has produced many severe plastic deformations in the CoCrMo alloy that caused a large number of dislocations and stacking faults [29]. These structural changes have induced numerous diffusion pathways for oxygen that quickly increased the subsurface oxygen content. Consequently, the SMAT process has promoted the formation of a dense passive layer at the surface of the CoCrMo alloy that improves the protection of the metallic implant against corrosion in an aggressive physiological solution.

Table 2 Corrosion parameters of the four samples obtained from the proposed model

CoCrMo sample	W	W-P	S15	S15-P
R_s (Ω cm^2)	42.4 ± 2.4	42.4 ± 2.4	40.1 ± 2.1	40.3 ± 2.1
C_f (μF cm^{-2})	14.8 ± 0.8	12.8 ± 0.7	6.0 ± 0.3	7.5 ± 0.4
R_f (kΩ cm^2)	313 ± 16	347 ± 18	722 ± 37	480 ± 24
R_{ct} (kΩ cm^2)	9.2 ± 0.5	9.8 ± 0.5	26.5 ± 1.4	11.3 ± 0.6
R_p (kΩ cm^2)	322 ± 17	357 ± 19	749 ± 39	491 ± 25
C_{dl} (μF cm^{-2})	674 ± 34	704 ± 36	106 ± 6	546 ± 28

Conclusion

In this study, the corrosion behavior of untreated and mechanically treated CoCrMo alloys was evaluated by potentiodynamic measurements and electrochemical impedance spectroscopy. These electrochemical studies reveal that the surface mechanical attrition treatment (SMAT) of the CoCrMo alloy by using 3-mm balls for 15 min promotes the passive film formation and increases the corrosion resistance during immersion in Ringer's solution. Indeed, after SMAT, the CoCrMo alloy shows a more positive corrosion potential and a lower corrosion current density. It is also shown that the specific biomedical polishing coupled with the SMAT process does not alter the advantages of the surface passivation generated by the SMAT.

References

1. KaivosojaE, TiainenVM, TakakuboY, RajchelB, SobieckiJ, KonttinenYT, TakagiM (2013) In: Affatato S (ed) Wear of orthopaedic implants and artificial joints, A volume in Woodhead Publishing Series in Biomaterials, Cambridge
2. Martin CT, Callaghan JJ, Gao Y, Pugely AJ, Liu SS, Warth LC, Goetz DD (2016) What can we learn from 20-year followup studies of hip replacement? Clin Orthop Relat Res 474(2):402–407. https://doi.org/10.1007/s11999-015-4260-7
3. Kamath AF, Sheth NP, Hosalkar HH, Babatunde OM, Lee GC, Nelson CL (2012) Modern total hip arthroplasty in patients younger than 21 years. J Arthroplast 27(3):402–408. https://doi.org/10.1016/j.arth.2011.04.042
4. Pezzotti G, Yamamoto K (2014) Artificial hip joints: the biomaterials challenge. J Mech Behav Biomed Mater 31:3–20. https://doi.org/10.1016/j.jmbbm.2013.06.001

5. Wang XH, Li JS, Hu R, Kou HC (2015) Mechanical properties and pore structure deformation behaviour of biomedical porous titanium. Trans Nonferrous Met Soc China 25(5):1543–1550. https://doi.org/10.1016/S1003-6326(15)63756-6
6. Niinomi M (2008) Metallic biomaterials. J Artif Organs 11(3):105–110. https://doi.org/10.1007/s10047-008-0422-7
7. Jaimes RFVV, Afonso MLCA, Rogero SO, Agostinho SML, Barbosa CA (2010) New material for orthopedic implants: electrochemical study of nickel free P558 stainless steel in minimum essential medium. Mater Lett 64(13):1476–1479. https://doi.org/10.1016/j.matlet.2010.03.066
8. Geetha M, Singh AK, Asokamani R, Gogia AK (2009) Ti based biomaterials, the ultimate choice for orthopaedic implants—a review. Prog Mater Sci 54(3):397–425. https://doi.org/10.1016/j.pmatsci.2008.06.004
9. Simon JP, Fabry G (1991) An overview of implants materials. Acta Orthop Belg 57(1):1–5
10. Jin L, Cui W, Song X, Liu G, Zhou L (2014) Effects of surface nanocrystallization on corrosion resistance of β-type titanium alloy. Trans Nonferrous Met Soc China 24(8):2529–2535. https://doi.org/10.1016/S1003-6326(14)63379-3
11. Liu G, Lu J, Lu K (2000) Surface nanocrystallization of 316L stainless steel induced by ultrasonic shot peening. Mater Sci Eng A 286(1):91–95. https://doi.org/10.1016/S0921-5093(00)00686-9
12. Liu G, Wang SC, Lou XF, Lu J, Lu K (2001) Low carbon steel with nanostructured surface layer induced by high-energy shot peening. Scripta Mater 44(8-9):1791–1795. https://doi.org/10.1016/S1359-6462(01)00738-2
13. Zhang K, Zhang X, Deng X, Li X, Ma M (2013) Relationship between extrusion, Y and corrosion behavior of Mg-Y alloy in NaCl solution. J Magnesium Alloys 1(2):134–138. https://doi.org/10.1016/j.jma.2013.07.002
14. Yang S, Dillon OW, Puleo D, Jawahir IS (2013) Effect of cryogenic burnishing on surface integrity modifications of Co-Cr-Mo biomedical alloy. J Biomed Mater Res B Appl Biomater 101B(1):139–152. https://doi.org/10.1002/jbm.b.32827
15. Ralston KD, Birbilis N, Davies CHJ (2010) Revealing the relationship between grain size and corrosion rate of metals. Scripta Mater 63(12):1201–1204. https://doi.org/10.1016/j.scriptamat.2010.08.035
16. Balusamy T, Sankara Narayanan TSN, Ravichandran K, Park IS, Lee MH (2013) Influence of surface mechanical attrition treatment (SMAT) on the corrosion behaviour of AISI 304 stainless steel. Corros Sci 74:332–344. https://doi.org/10.1016/j.corsci.2013.04.056
17. Hao YW, Deng B, Zhong C, Jiang YM, Li J (2009) Effect of surface mechanical attrition treatment on corrosion behavior of 316 stainless steel. J Iron Steel Res Int 16(2):68–72. https://doi.org/10.1016/S1006-706X(09)60030-3
18. Balusamy T, Kumar S, Sankara Narayanan TSN (2010) Effect of surface nanocrystallization on the corrosion behaviour of AISI 409 stainless steel. Corros Sci 52(11):3826–3834. https://doi.org/10.1016/j.corsci.2010.07.004
19. Jelliti S, Richard C, Retraint D, Roland T, Chemkhi M, Demangel C (2013) Effect of surface nanocrystallization on the corrosion behavior of Ti-6Al-4V titanium alloy. Surf Coat Technol 224:82–87. https://doi.org/10.1016/j.surfcoat.2013.02.052
20. Petrov YN, Prokopenko GI, Mordyuk BN, Vasylyev MA, Voloshko SM, Skorodzievski VS, Filatova VS (2016) Influence of microstructural modifications induced by ultrasonic impact treatment on hardening and corrosion behavior of wrought Co-Cr-Mo biomedical alloy. Mater Sci Eng C 58:1024–1035. https://doi.org/10.1016/j.msec.2015.09.004
21. Demangel C, Poznanski A, Steenhout V, Levesque A, Benhayoune H, Retraint D (2014) Benefit of a surface nanocrystallization treatment on Co28Cr6Mo abrasive wear properties. Adv Mater Res 966–967:435–441. https://doi.org/10.4028/www.scientific.net/AMR.966-967.435
22. Zhang LC, Kiat ECS, Pramanik A (2009) A briefing on the manufacture of hip joint prostheses. Adv Mater Res 76-78:212–216. https://doi.org/10.4028/www.scientific.net/AMR.76-78.212
23. Lu K, Lu J (2004) Nanostructured surface layer on metallic materials induced by surface mechanical attrition treatment. Mat Sci Eng A 375–377:38–45
24. Yamanaka K, Mori M, Kurosu S, Matsumoto H, Chiba A (2009) Ultrafine grain refinement of biomedical Co-29Cr-6Mo alloy during conventional hot-compression deformation. Metall Mater Trans A 40(8):1980–1994. https://doi.org/10.1007/s11661-009-9879-0
25. Drevet R, Aaboubi O, Benhayoune H (2012) In vitro corrosion behavior of electrodeposited calcium phosphate coatings on Ti6Al4V substrates. J Solid State Electrochem 16(9):3069–3077. https://doi.org/10.1007/s10008-012-1742-3
26. Wu X, Tao N, Hong Y, Liu G, Xu B, Lu J, Lu K (2005) Strain-induced grain refinement of cobalt during surface mechanical attrition treatment. Acta Mater 53(3):681–691. https://doi.org/10.1016/j.actamat.2004.10.021
27. McCafferty E (2005) Validation of corrosion rates measured by the Tafel extrapolation method. Corros Sci 47(12):3202–3215. https://doi.org/10.1016/j.corsci.2005.05.046
28. Fu T, Zhan Z, Zhang L, Yang Y, Liu Z, Liu J, Li L, Yu X (2015) Effect of surface mechanical attrition treatment on corrosion resistance of commercial pure titanium. Surf Coat Technol 280:129–135. https://doi.org/10.1016/j.surfcoat.2015.08.041
29. Luo H, Dong CF, Xiao K, Li XG (2011) Characterization of passive film on 2205 duplex stainless steel in sodium thiosulphate solution. Appl Surf Sci 258(1):631–639. https://doi.org/10.1016/j.apsusc.2011.06.077
30. Li H, Jiang Z, Feng H, Wang Q, Zhang W, Fan G, Li G, Wang L (2015) Electrochemical corrosion characteristics of super duplex stainless steel S32750 in LT-MED environment. Int J Electrochem Sci 10:1616–1631